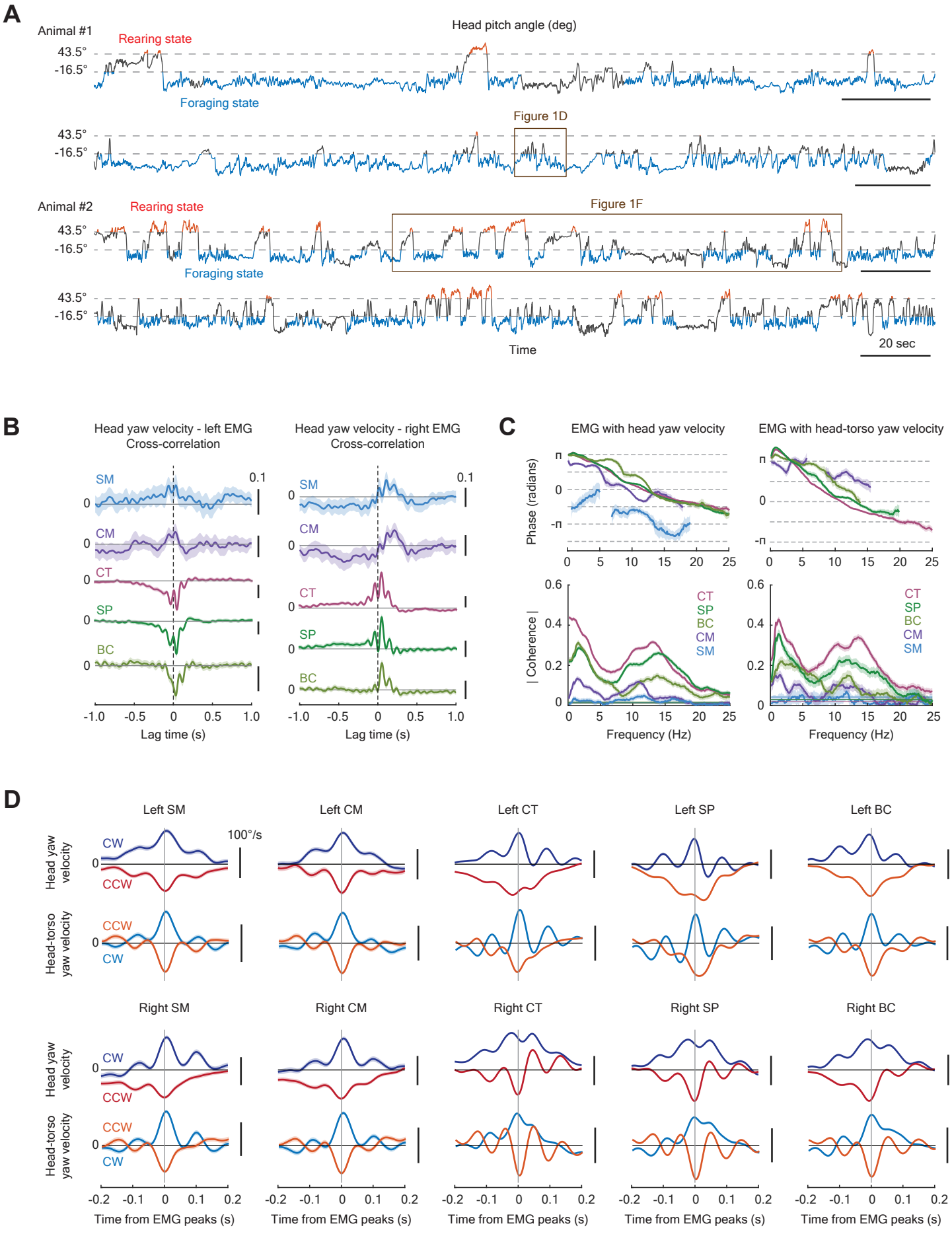

Figure S1. Liao and Kleinfeld (updated 15 Aug 2022)

Figure S1: Behavior classification and control of head movements with neck muscles. Related to Figure 3.

(A) Classification of foraging and rearing states in freely moving rats. Data from two rats. Dashed lines show the lower boundary (43.5°) for defining the rearing state and the upper boundary (-16.5°) for defining the foraging state. Black traces are the data that do not reside in the foraging and rearing states or that are miscellaneous behaviors (scratching, grooming, etc., see Star Methods).

(B) Correlation with head yaw velocity with neck muscle EMGs. Error bars are standard errors. Data from individual rats in the foraging state (window size = 4 s, SM and CM: 34, CT: 152, SP and BC: 144 segments)

(C) (Left) Coherence of neck EMGs with head yaw velocity. Data pooled from multiple rats in the foraging state (SM: 7, CM: 8, CT: 11, SP: 10, BC: 7 rats), using window size = 4 s, half-bandwidth = 1 Hz, 7 tapers (SM: 1803, CM: 2039, CT: 3013, SP: 2557, BC: 1435 segments). **(Right)** Coherence of neck EMGs with head-torso yaw velocity. Data pooled from multiple rats in the foraging state (SM: 2, CM: 3, CT: 4, SP: 3, BC: 3 rats), using window size = 4 s, half-bandwidth = 1 Hz, and 7 tapers (SM: 236, CM: 501, CT: 1063, SP and BC: 488 segments). Error bars are standard errors (jackknife). Horizontal lines indicate 95% confidence levels.

(D) Correlation of head/head-torso yaw velocity with respect to neck EMG peaks. Clockwise (CW) and counterclockwise (CCW) head-scans, defined at the time of the EMG peak, are plotted separately. Data from individual rats in the foraging states. All y-axes plotted to the same scale. Error bars are standard errors.

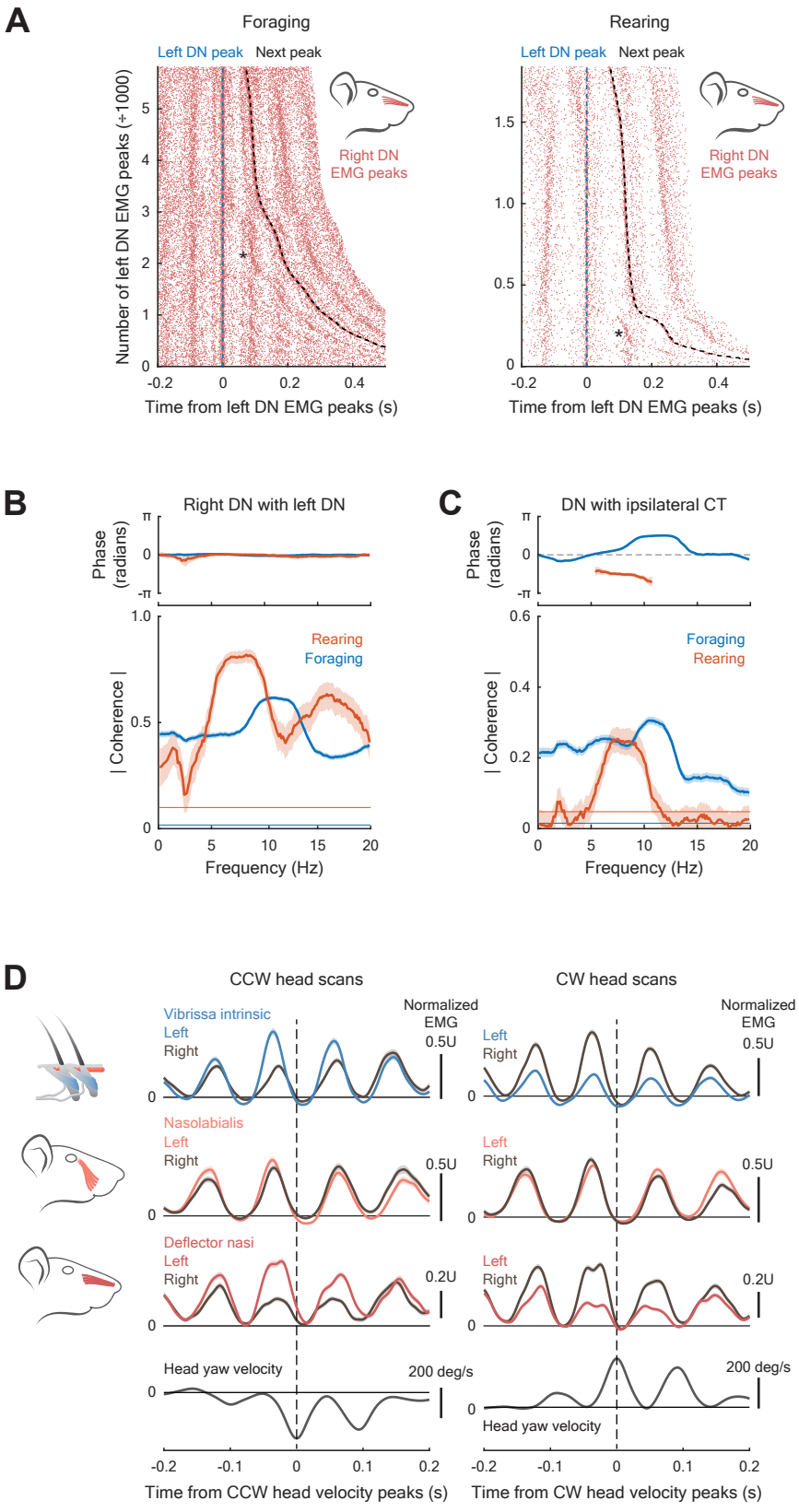

Figure S2. Liao and Kleinfeld (updated 23 November 2022)

Figure S2: Coordination between orofacial motor plants. Related to Figure 5.

(A) Raster plots of the right DN EMG peaks with respect to the left DN EMG peaks in the foraging (left) and rearing (right) states. Asterisks mark unilateral activation of DN muscle. Data from one rat.

(B) Coherence of the right DN with the left DN EMG envelopes. Data from three rats. The horizontal lines indicate the 95 % confidence levels. The trial size = 4 s and we used 15 tapers for a half-bandwidth of 2 Hz. We used 692 trials for foraging and 20 for rearing.

(C) Coherence of the left DN with the left CT EMG envelopes. Data from three rats. The trial size = 4 s and we used 15 tapers for a half-bandwidth of 2 Hz. We used 842 trials for foraging and 87 for rearing. The jackknife errors are shown. The horizontal lines indicate the 95 % confidence levels.

(D) Cross-correlation of the normalized EMG envelopes of VI, NL, and DN with respect to the counterclockwise (left) and clockwise (right) peaks in the head yaw velocity. For each EMG record, the 50-th percentile is set to be zero and the data was normalized so the 10-th to 90-th percentile have a difference of one unit. The head-yaw velocity recorded along with the example VI and DN data is also shown (bottom).

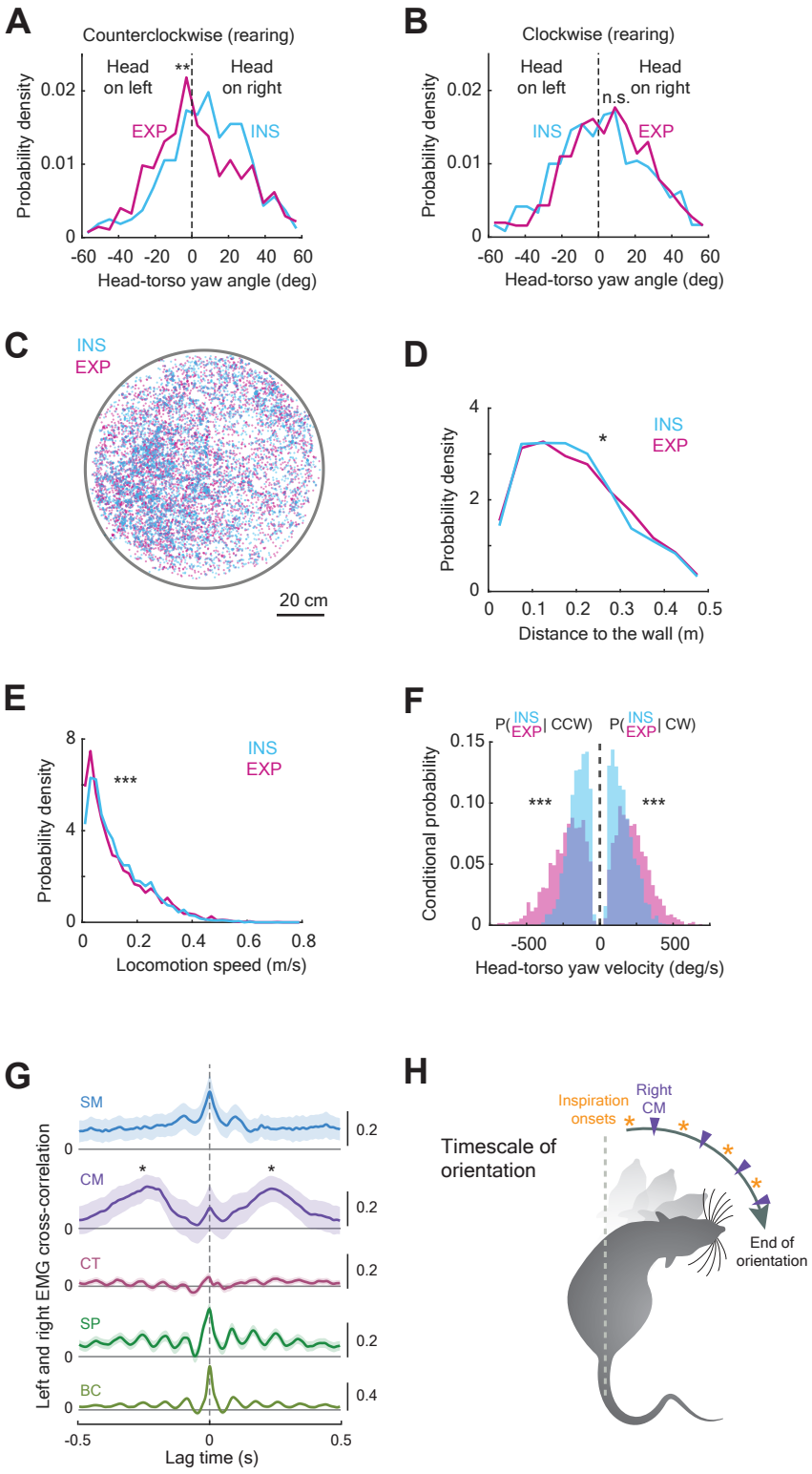

Figure S3. Liao and Kleinfeld (23 November 2022)

Figure S3: Bimodal head scanning and head orientation. Related to Figure 6.

In all panels, INS (and EXP) head-scans are defined for the head-torso yaw velocity peaks that lie in the range of the phases [0.05π, 0.55π] radians, and [1.1π, 1.6π] radians, in the sniffing cycles, i.e., 6 - 10 Hz in panels A-B, and 8 - 14 Hz in panels C-F.

(A) Probability density distribution of the instantaneous head-torso yaw angle of inspiratory (INS) and expiratory (EXP) counterclockwise head scans during the rearing state ($p = 0.0013$, Kolmogorov-Smirnov test).Number of INS/EXP head scans: 269/458. Data pooled from 17 rats.

(B) Probability density distribution of the instantaneous head-torso yaw angle of inspiratory (INS) and expiratory (EXP) clockwise head scans during the rearing state ($p = 0.1644$, Kolmogorov-Smirnov test). Number of INS/EXP head scans: 400/424. Data pooled from 17 rats.

(C) The scatter plot of the location in the arena where a rat performs inspiratory (INS) or expiratory (EXP) head scans. Data from one rat.

(D) Probability density of the occurrence of INS and EXP head scans as a function of the instantaneous distance to the arena wall. Data from one rat.

(E) Probability density of the occurrence of INS and EXP head scans as a function of the instantaneous locomotion speed. Locomotion speed is calculated by taking the time derivative of the video tracking data. Data from one rat.

(F) Conditional probability of INS and EXP head scans in clockwise (prob(INS|CW) and prob(EXP|CW)) or counterclockwise head-scans (prob(INS|CCW) and prob(EXP|CCW)), as a function of the instantaneous head-torso yaw speed. Data from one rat.

(G) Cross-correlation of left and right neck EMG signals in the foraging state, averaged from segments of length 4 s. Data from individual rats (SM and CM: 34 segments, CT: 152 segments, SP and BC: 144 segments). Error bars are standard errors. Asterisks mark the activities related to head orientation.

(H) Illustration of the activation pattern of CM in head orientation.

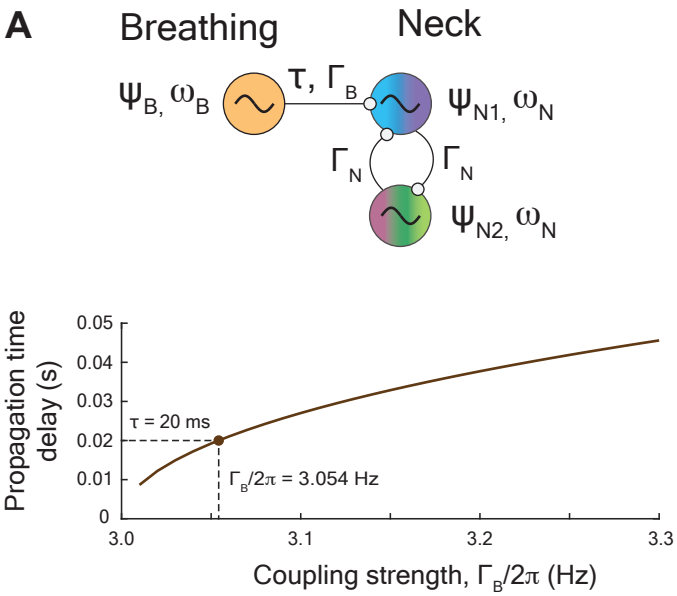

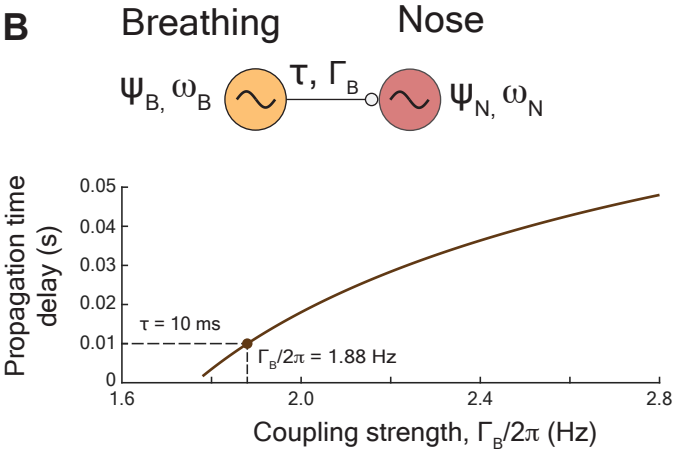

Figure S4. Liao and Kleinfeld (updated 18 December 2022)

Figure S4: Computational models for phase shifts. Related to Figure 7.

(A) Unidirectional coupling model for head movement. We plot propagation time delay as a function of the coupling strength that can generate a phase shift of π radians across states.

(B) Unidirectional coupling model for nose twitching. Propagation time delay as a function of the coupling strength that can generate a phase shift of 0.65π radians across states.

Table S1. Electromyogram (EMG) recordings in each animal.

#	ID	SM	CM	CT	SP	BC	VI	NL	DN	Torso sensor
1	SLR087									X
2	SLR089									X
3	SLR090									X
4	SLR092									X
5	SLR093									X
6	SLR094				L + R					
7	SLR095									X
8	SLR096			L + R	L + R					
9	SLR097			L + R	L + R					
10	SLR099						L	L + R	R	
11	SLR100								L + R	
12	SLR102			L + R						X
13	SLR103			L + R						X
14	SLR105			L + R						X
15	SLR106			L + R						X
16	SLR107		L + R							
17	SLR108		L + R							X
18	SLR110	L + R	L + R							X
19	SLR111	L + R	L + R							X
20	SLR112				L + R	L + R				X
21	SLR113				L + R	L + R				X
22	SLR114	L + R								
23	SLR115				L + R	L + R				X
24	SLR116						L + R		L + R	
25	SLR117						L + R		L + R	
26	SLR119	L	L	L	L					X
27	SLR120			L	L	L			L	
28	SLR121			L	L	L			L	
29	SLR122	L	L	L					L	
30	SLR123	L	L	L		L				
31	SLR124	L	L		L	L				
32	SLR125						L + R	L + R		
33	SLR126						L + R	L + R		

L: Left muscle. R: Right muscle. SM: Sternomastoid. CM: Cleidomastoid. CT: Clavotrapezius. SP: Splenius. BC: Biventer Cervicis. VI: Vibrissa Intrinsic. NL: Nasolabialis. DN: Deflector nasi.

Table S1. Electromyogram (EMG) recordings in each animal. Related to Figure 3.

In all animals, thermocouple and head orientation sensor are implanted. L: Left muscle. R: Right muscle. SM: Sternomastoid. CM: Cleidomastoid. CT: Clavotrapezius. SP: Splenius. BC: Biventer Cervicis. VI: Vibrissa Intrinsic. NL: Nasolabialis. DN: Deflector nasi.